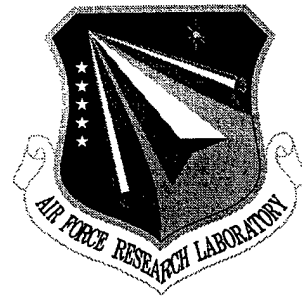


AFRL-SN-RS-TR-1998-104
Final Technical Report
June 1998



**DEVELOPMENT OF NOVEL, BAND-GAP
ENGINEERED PHOTOREFRACTIVE SEMI-
CONDUCTORS CdMnTe:V FOR REAL TIME
OPTICAL PROCESSING**

Brimrose Corporation of America

**S. B. Trivedi, G. V. Jagannathan, S. W. Kutcher, K. Grasza, Z. Yu,
R. D. Rosemeier, and R. Scheerer**

APPROVED FOR PUBLIC RELEASE; DISTRIBUTION UNLIMITED.

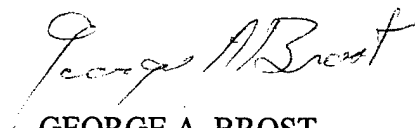
19980702 132

**AIR FORCE RESEARCH LABORATORY
SENSORS DIRECTORATE
ROME RESEARCH SITE
ROME, NEW YORK**

This report has been reviewed by the Air Force Research Laboratory, Information Directorate, Public Affairs Office (IFOIPA) and is releasable to the National Technical Information Service (NTIS). At NTIS it will be releasable to the general public, including foreign nations.

AFRL-SN-RS-TR-1998-104 has been reviewed and is approved for publication.

APPROVED:



GEORGE A. BROST
Project Engineer

FOR THE DIRECTOR:



ROBERT G. POLCE, Acting Chief
Rome Operations Office
Sensors Directorate

If your address has changed or if you wish to be removed from the Air Force Research Laboratory Rome Research Site mailing list, or if the addressee is no longer employed by your organization, please notify AFRL/SNDR, 25 Electronic Pky, Rome, NY 13441-4515. This will assist us in maintaining a current mailing list.

Do not return copies of this report unless contractual obligations or notices on a specific document require that it be returned.

REPORT DOCUMENTATION PAGE			Form Approved OMB No. 0704-0188	
Public reporting burden for this collection of information is estimated to average 1 hour per response, including the time for reviewing instructions, searching existing data sources, gathering and maintaining the data needed, and completing and reviewing the collection of information. Send comments regarding this burden estimate or any other aspect of this collection of information, including suggestions for reducing this burden, to Washington Headquarters Services, Directorate for Information Operations and Reports, 1215 Jefferson Davis Highway, Suite 1204, Arlington, VA 22202-4302, and to the Office of Management and Budget, Paperwork Reduction Project (0704-0188), Washington, DC 20503.				
1. AGENCY USE ONLY (Leave blank)	2. REPORT DATE June 1998	3. REPORT TYPE AND DATES COVERED FINAL Jul 95 - Jul 96		
4. TITLE AND SUBTITLE DEVELOPMENT OF NOVEL, BAND-GAP ENGINEERED PHOTOREFRACTIVE SEMICONDUCTORS CdMnTe:V FOR REAL TIME OPTICAL PROCESSING		5. FUNDING NUMBERS C - F30602-95-C-0154 PE - 62702F PR - 4600 TA - P4 WU - PV		
6. AUTHOR(S) S.B. Trivedi, G.V. Jagannathan, S.W. Kutcher, K. Grasza, Z. Yu, R.D. Rosemeier, R. Scheerer				
7. PERFORMING ORGANIZATION NAME(S) AND ADDRESS(ES) Brimrose Corporation of America 5024 Campbell Blvd, Ste E Baltimore MD 21236		8. PERFORMING ORGANIZATION REPORT NUMBER N/A		
9. SPONSORING/MONITORING AGENCY NAME(S) AND ADDRESS(ES) Air Force Research Laboratory/SNDR 25 Electronic Pky Rome NY 13441-4515		10. SPONSORING/MONITORING AGENCY REPORT NUMBER AFRL-SN-RS-TR-1998-104		
11. SUPPLEMENTARY NOTES Project Engineer: George Brost, AFRL/SNDR, (315) 330-7669				
12a. DISTRIBUTION AVAILABILITY STATEMENT APPROVED FOR PUBLIC RELEASE: DISTRIBUTION UNLIMITED			12b. DISTRIBUTION CODE	
13. ABSTRACT (Maximum 200 words) During this project, we have developed and produced application quality photorefractive Cd _{1-x} MnxTe:V crystals with compositions x= 0.15, 0.45, and 0.60. These crystals are useful for applications in the wavelength range of 0.7 to 1.3mm. These crystals were obtained through the following material processing steps: (1) extensive purification of the starting elements (cadmium, manganese and tellurium) and purification of the compound (Cd _{1-x} MnxTe); (2) crystal growth from the melt under controlled conditions of heat and mass transfers; and (3) in situ annealing of the crystals after growth. The optimal temperature profile required to produce a favorable growth interface and minimal stress for crystals grown by the Bridgman-Stockbarger method was determined. From computational models, the temperature distribution within the solid and melt in the growth ampoule was calculated and used to construct an improved experimental system for growth of high quality Cd _{1-x} MnxTe:V single crystals.				
14. SUBJECT TERMS Photorefraction, CdMnTe			15. NUMBER OF PAGES 40	
			16. PRICE CODE	
17. SECURITY CLASSIFICATION OF REPORT UNCLASSIFIED	18. SECURITY CLASSIFICATION OF THIS PAGE UNCLASSIFIED	19. SECURITY CLASSIFICATION OF ABSTRACT UNCLASSIFIED	20. LIMITATION OF ABSTRACT UL	

**DEVELOPMENT OF NOVEL, BAND-GAP ENGINEERED
PHOTOREFRACTIVE SEMICONDUCTORS CdMnTe:V FOR
REAL TIME OPTICAL PROCESSING**

Table of Contents

1.0	Executive Summary	1
2.0	Introduction	2
3.0	Crystal Growth	3
3.1	Purification and Synthesis	4
3.2	Construction of Experimental Crystal Growth System	4
3.3	Crystal Growth using Experimental System	5
3.4	Evaluation of Experimental Crystal Growth System	6
4.0	Crystal Characterization	9
4.1	Electrical Measurements	10
4.2	Magneto-optic and Absorption Measurements	12
4.3	Photoluminescence Measurements	16
4.4	Absorption and Emission Measurements	18
4.5	Infrared Microscopy	21
4.6	Photorefractive Characterization	25
5.0	Conclusions and Possible Future Work	25
6.0	References	26

**DEVELOPMENT OF NOVEL, BAND-GAP ENGINEERED
PHOTOREFRACTIVE SEMICONDUCTORS CdMnTe:V FOR
REAL TIME OPTICAL PROCESSING**

List of Tables/Figures

TABLES

Table I	Calculated values of attenuation and magneto-optic parameters at $\lambda = 632.8\text{nm}$ for 2 samples of $\text{Cd}_{0.55}\text{Mn}_{0.45}\text{Te:V}$ and an annealed sample of $\text{Cd}_{0.55}\text{Mn}_{0.45}\text{Te:V}$	15
---------	--	----

FIGURES

1	Schematic of experimental growth system	6
2	Photograph of $\text{Cd}_{0.85}\text{Mn}_{0.15}\text{Te:V}$	7
3	Temperature distribution computed along the axis of the charge/ampoule interface	8
4	I-V characteristics for $\text{Cd}_{0.55}\text{Mn}_{0.45}\text{Te:V}$	11
5	Conductivity of $\text{Cd}_{0.85}\text{Mn}_{0.15}\text{Te:V}$	12
6	Apparatus used to measure polarization rotation	13
7	Absorption coefficient versus wavelength for $\text{Cd}_{0.55}\text{Mn}_{0.45}\text{Te}$	15
8	Photoluminescence spectrum of $\text{Cd}_{0.55}\text{Mn}_{0.45}\text{Te}$	16
9	Photoluminescence spectrum of $\text{Cd}_{0.55}\text{Mn}_{0.45}\text{Te:V}$	17

10	Absorption spectrum of $\text{Cd}_{0.85}\text{Mn}_{0.15}\text{Te:Cr}$	18
11	Emission spectrum of $\text{Cd}_{0.85}\text{Mn}_{0.15}\text{Te:Cr}$ at various temperatures using an argon ion laser (488nm) as the excitation source	19
12	Emission spectrum of $\text{Cd}_{0.85}\text{Mn}_{0.15}\text{Te:Cr}$ at various temperatures using a 790nm diode laser as the excitation source	20
13	Integrated emission intensity versus temperature for $\text{Cd}_{0.85}\text{Mn}_{0.15}\text{Te:Cr}$	21
14	IR microscope picture of $\text{Cd}_{0.55}\text{Mn}_{0.45}\text{Te:V}$	22
15	IR microscope picture of $\text{Cd}_{0.85}\text{Mn}_{0.15}\text{Te:V}$	23
16	IR microscope pictures of as-grown (top) and annealed (bottom) $\text{Cd}_{0.40}\text{Mn}_{0.60}\text{Te}$	24

**DEVELOPMENT OF NOVEL, BAND-GAP ENGINEERED
PHOTOREFRACTIVE SEMICONDUCTORS CdMnTe:V FOR
REAL TIME OPTICAL PROCESSING**

Acknowledgments

This research was supported by The United States Air Force. This program was monitored by Dr. George Brost of Rome Laboratory, Griffiss Air Force Base. We thank Dr. Brost for his constant interest, support and scientific input during this research work.

We would also like to thank Dr. James Kennedy of the CECOM Night Vision and Electronics Sensors Directorate at Fort Belvoir, Virginia for providing the infrared microscope that was used to photograph the crystals, and Dr. C.C. Wang of NEC Research Institute in Princeton, New Jersey for the conductivity and mobility-lifetime measurements.

We thank Ms. Miriam Brown of Brimrose Corporation for her valuable help in orienting, cutting, and polishing of the crystals.

Finally, the excellent support of Diane Murray for contract administration and preparation of this report is gratefully acknowledged.

Development of Novel, Band-Gap Engineered Photorefractive Semiconductors CdMnTe:V for Real Time Optical Processing

1.0 Executive Summary

During this project, we have developed and produced application quality photorefractive $\text{Cd}_{1-x}\text{Mn}_x\text{Te:V}$ crystals with compositions $x=0.15, 0.45$ and 0.60 . These crystals are useful for applications in the wavelength range of 0.7 to $1.3\mu\text{m}$. These crystals were obtained through the following material processing steps:

- (1) extensive purification of the starting elements (cadmium, manganese and tellurium) and purification of the compound ($\text{Cd}_{1-x}\text{Mn}_x\text{Te}$);
- (2) crystal growth from the melt under controlled conditions of heat and mass transfers; and
- (3) in situ annealing of the crystals after growth.

The optimal temperature profile required to produce a favorable growth interface and minimal stress for crystals grown by the Bridgman-Stockbarger method was determined. From computational models, the temperature distribution within the solid and melt in the growth ampoule was calculated and used to construct an improved experimental system for growth of high quality $\text{Cd}_{1-x}\text{Mn}_x\text{Te:V}$ single crystals.

These crystals were characterized using a variety of techniques. The $\text{Cd}_{1-x}\text{Mn}_x\text{Te:V}$ crystals were found to be highly resistive, with resistivity on the order of 10^8 to 10^{10} $\Omega\text{-cm}$, and highly photoconductive. The magneto-optic and absorption measurements indicated that $\text{Cd}_{0.55}\text{Mn}_{0.45}\text{Te:V}$ is a suitable material for high quality magneto-optic device applications at wavelengths less than $1\mu\text{m}$, with properties superior to those of previously reported materials. Photoluminescence, absorption and emission measurements were performed and the results were used to analyze the band structure and overall quality of the crystals. Infrared microscopy was used to examine the bulk structure of $\text{Cd}_{0.85}\text{Mn}_{0.15}\text{Te:V}$ and $\text{Cd}_{0.55}\text{Mn}_{0.45}\text{Te:V}$, and to compare the crystal structure of as-grown and annealed $\text{Cd}_{0.40}\text{Mn}_{0.60}\text{Te:V}$ crystals. We found that high temperature annealing had a profound effect on the quality of $\text{Cd}_{0.40}\text{Mn}_{0.60}\text{Te:V}$ crystals and can be used to enhance its usefulness.

The transmission spectrum, two beam coupling gain coefficient and grating time constant for $\text{Cd}_{0.55}\text{Mn}_{0.45}\text{Te:V}$ were also investigated. Photorefractive two-beam coupling was observed from 0.63 to $1.3\mu\text{m}$. The photorefractive gain under diffusion conditions at $0.75\mu\text{m}$ and a $1\mu\text{m}$ grating

period was 0.4cm^{-1} and the effective trap concentration was calculated to be about $1.2 \times 10^{15}\text{cm}^{-3}$. The absorption coefficient at 0.75mm was 2.3cm^{-1} . A photorefractive gain as high as 5.6cm^{-1} at 15mm grating period with square wave ac fields of 7kV/cm was observed, and the value of the electro-optic coefficient at 0.75mm was measured to be 2.8 pm/V . Additionally, we observed electron-hole competition in crystals prepared at Brimrose for the first time.

2.0 Introduction

A current need exists for photorefractive materials operating at near infrared wavelengths which are compatible with semiconductor lasers. To the best of our knowledge, Brimrose has been the only company in the country to develop photorefractive semiconductors like CdTe:V [1,2], ZnTe:V [3,4], and $\text{Cd}_{1-x}\text{Zn}_x\text{Te:V}$ [4] operating at near infrared wavelengths. During this project, we investigated the development of the novel photorefractive semiconductor $\text{Cd}_{1-x}\text{Mn}_x\text{Te:V}$.

$\text{Cd}_{1-x}\text{Mn}_x\text{Te}$ belongs to a group of materials known as dilute magnetic semiconductor (DMS's) in which atoms of the group II element of the II-VI compound are randomly replaced by magnetic Mn^{++} ions. The semiconducting and structural properties such as band gap and lattice parameter can be controlled by varying the composition of the alloy. DMS alloys exhibit several very interesting magnetic properties related to the presence of the manganese. These properties include spin-glass transition, antiferromagnetic cluster formation, magnon excitations and enhancement of the electronic g-factor. As a result of these magnetic properties, these materials are useful in a number of device applications such as magnetic field tuned sources, optical phase shifters, Faraday rotation based magnetometers and high efficiency solar cells. $\text{Cd}_{1-x}\text{Mn}_x\text{Te:V}$, in particular, has shown usefulness for applications such as dynamic holography, laser power beam-combining optical correlation and acousto optic signal processing.

There has also been considerable work recently in the photorefractive properties of these materials. Initially, efforts in this direction focused on CdTe . It was determined that CdTe displayed photorefractivity when near-mid-gap (deep) levels were introduced into the band structure. Several methods of introducing these defect or impurity centers were investigated, and results indicated that doping CdTe with transition elements such as scandium, titanium and vanadium was the most suitable way or introducing these deep energy levels.

Photorefractive $\text{Cd}_{1-x}\text{Mn}_x\text{Te:V}$ was recently developed and produced by Brimrose Corporation in collaboration with Rome Laboratories (Dr. George Brost, OCPA). This material was found to operate at room temperature at visible and near infrared wavelengths with good figures of merit. A photorefractive gain of 0.5cm^{-1} was observed in $\text{Cd}_{0.55}\text{Mn}_{0.45}\text{Te:V}$ at a wavelength of 0.75mm [5-9].

Several material parameters are necessary for photorefractivity. Efficient photoconductivity is a prerequisite for the photorefractive process and affects the saturation intensity, the efficiency and the speed of non-linearity. Both the resistivity and photoconductivity of a photorefractive material depends on the transport properties, mobility and carrier lifetime. The ability to write an

efficient grating at low intensity levels requires a large dark resistivity. In an ideal undoped crystal at a given temperature, mobility is dependent on the effective carrier mass and optical-phonon structure. In the case of intrinsically or extrinsically doped 'non-ideal' crystals, both the mobility and lifetime depend upon the physical and chemical imperfections in the crystal. A reduction in these imperfections can improve the transport properties of the crystal. In order to induce photorefractivity in II-VI compound semiconductors, doping with transition element impurities is required. The mobility and lifetime decreases with the increasing concentration of deep levels. To obtain photorefractive gain and diffraction efficiency useful for device applications, the concentration of 'active' deep levels must be in the range 10^{15} to 10^{16} cm^{-3} [1,5,8]

It was recently reported that the second harmonic non-linear optical coefficient, d_{14} , of $\text{Cd}_{1-x}\text{Mn}_x\text{Te}$ was much greater than that of pure CdTe [10]. The coefficient peaks in the range of x from 0.2 to 0.5 where it is about twice as large as the coefficient for CdTe. Since the d_{14} coefficient and the electro-optic coefficient, r_{41} , are caused by the same physical phenomena, one can expect a corresponding increase in the electro-optic coefficient of $\text{Cd}_{1-x}\text{Mn}_x\text{Te}$ compared to CdTe. The increase may differ however, because of the dispersion of the indices of refraction of the material. The measurement of the electro-optic coefficient involves one low frequency which is typically below the infrared bands of the material, and the dispersion at this low frequency will affect the magnitude of the electro-optic effect. One must therefore measure the electro-optic coefficient to determine the magnitude of the increase over CdTe.

Experimental results have shown that the electro-optic coefficient of $\text{Cd}_{1-x}\text{Mn}_x\text{Te}$ is less than that of CdTe. Possible reasons for this include: anisotropy in crystalline structure, strain induced birefringence, or other material parameters.

Therefore, during this project, we worked to obtain application quality photorefractive crystals of $\text{Cd}_{1-x}\text{Mn}_x\text{Te}:\text{V}$ with a minimum concentration of intrinsic and extrinsic point defects, dislocation densities and twins.

3.0 Crystal Growth

$\text{Cd}_{1-x}\text{Mn}_x\text{Te}$ crystallizes in the zinc blende structure for values of x up to 0.77. The temperature versus composition phase diagram of CdTe-MnTe shows a coincidence of the solidus and liquidus lines. This coincidence leads to very little phase separation upon cooling. Thus, single phase $\text{Cd}_{1-x}\text{Mn}_x\text{Te}$ crystals with reasonably good homogeneity can be grown from the melt.

During this project, extensive efforts were made to improve upon the methods currently used for growth of $\text{Cd}_{1-x}\text{Mn}_x\text{Te}$ crystals. Based on computational models as well as experimental investigations, we constructed an improved crystal growth system. Using this experimental system, we were able to grow high quality vanadium doped $\text{Cd}_{1-x}\text{Mn}_x\text{Te}$ crystals with compositions $x=0.45$, 0.15 and 0.00. The following sections describe the purification and synthesis of the constituent elements, the construction of the experimental growth system, the process of crystal growth and an evaluation of this system.

3.1 Purification and Synthesis

Extensive purification of the constituent elements, cadmium, manganese, and tellurium was carried out. The purity of the starting cadmium and tellurium was 99.9999% and the manganese was 99.98%. These elements were further purified by repeated vacuum sublimation. The dopant elements, chromium and vanadium, were purified via chemical cleaning.

For synthesis of CdMnTe, the purified starting materials were carefully weighed in correct stoichiometric proportions and placed in graphitized fused silica ampoules (approximately 20cm long and 20mm in diameter). For the doped crystals, chromium or vanadium was added so that the starting concentration of the dopant was 1×10^{19} atoms/cm³. After being vacuum sealed, the ampoules were placed in a three zone Bridgman furnace. The temperature of the furnace was controlled as follows: 1) increased up to 600°C in two hours and held constant for 12 hours; 2) increased to 1125°C over 24 hours; 3) held constant and allowed to react and mix for 24 hours; 4) decreased to room temperature over a 24 hour period. The synthesized ingots were removed and cleaned in a bromine in methanol solution, resealed under vacuum in graphitized fused silica ampoules, and used for crystal growth via the Bridgman-Stockbarger technique.

3.2 Construction of Experimental Crystal Growth System

The shape of the solid-liquid interface is an important factor affecting the quality of crystals. However, it is the temperature distribution within the crystal rather than the interface shape that is the key factor governing thermal stress [11]. Thermal stress, which can generate dislocations, is generally minimal for planar isotherms. The maximum shear stress values appear on the outside layers of the crystal, especially near points of discontinuities in the temperature gradient in the Bridgman - Stockbarger configuration [12,13]. Additionally, the coldest end of the crystal is usually subjected to a relatively high radial temperature gradient. Minimizing the radial temperature gradients in the solidified portion of the material must be performed during growth along with maintaining a solid/liquid interface that is convex to the liquid. Therefore, the construction of an appropriate growth system is not a trivial task and demands close examination of the system by computer modeling as well as experimental investigations.

We designed a model for our Bridgman system and applied this model in the computational analysis [14]. In this model, the outside of the Cd_{1-x}Mn_xTe absorbs a fraction of the radiation that is transmitted by the quartz ampoule, and a portion of the radiation is absorbed by the quartz ampoule. The radiation that reaches the surfaces depends on the orientation of that particular surface. For the top and bottom surfaces the radiation view factors were calculated. For a vertical surface a Christiansen formula was used [11].

In the computational model, elements of the real experimental system were considered. The quartz ampoule was 17cm long, 1.5mm thick with a 2.5cm inner diameter. The Cd_{1-x}Mn_xTe charge was 10cm long, and the growth velocity was kept between 0.6 and 1.5mm/hour. The heat conduction coefficients used for calculation were similar to those used by Steer et.al. [15] for CdTe:

liquid $\text{Cd}_{1-x}\text{Mn}_x\text{Te}$ 2.2[W/K/m], solid $\text{Cd}_{1-x}\text{Mn}_x\text{Te}$ 1.1[W/K/m] and quartz 2.7[W/K/m]. Very weak convection was assumed. The furnace considered in the computations had a diameter of 3.5cm and had no radiation baffles. The temperature profile of the experimental furnace was measured near the wall in the presence of the loaded ampoule. The real furnace consisted of three independent 10cm diameter zones which were separated by 1cm thick radiation baffles.

3.3 Crystal Growth using Experimental System

Crystal growth was performed in a vertical three zone furnace. The material used for the growth of single crystals was obtained from the middle part of the synthesized ingots. All solidification processes were performed with great care to obtain single crystals. Ampoules prepared for growth of material comprising manganese were carbonized. The temperature of the material enclosed in the sealed ampoule was first slowly (in 48 hours) increased up to temperatures exceeding the melting point by 40-50°C. The melting point for CdTe was assumed to be 1092°C and that for $\text{Cd}_{0.55}\text{Mn}_{0.45}\text{Te}$ was assumed to be 1072°C [16]. The temperature in the three heating zones was either kept the same, or the temperature of the middle zone was 20°C higher than the temperature of the bottom and top zones (Figure 1). The molten material was subjected for 24 hours to an inverse temperature gradient (heating from below) in order to force mixing and homogenization of the material. The final change of the furnace temperature profile took up to 100 hours before pulling of the ampoule began, and growth was completed by linearly cooling the system for 24 hours. During the last stage of cooling, the temperature gradient was again inverted in order to prevent solidification of the excessive element (usually cadmium) in the slit between the crystal and ampoule wall. The stability of the temperature field close to the growth interface was carefully controlled and variation was determined to be less than 1°C. The temperature measured close to the growth interface increased systematically during the course of growth to 7-10°C above the temperature measured at the beginning of the growth. This effect is believed to result from the change in position of the ampoule. The temperature of the furnace wall was stabilized by independent controllers and control thermocouples were located in the middle part of the heating zones.

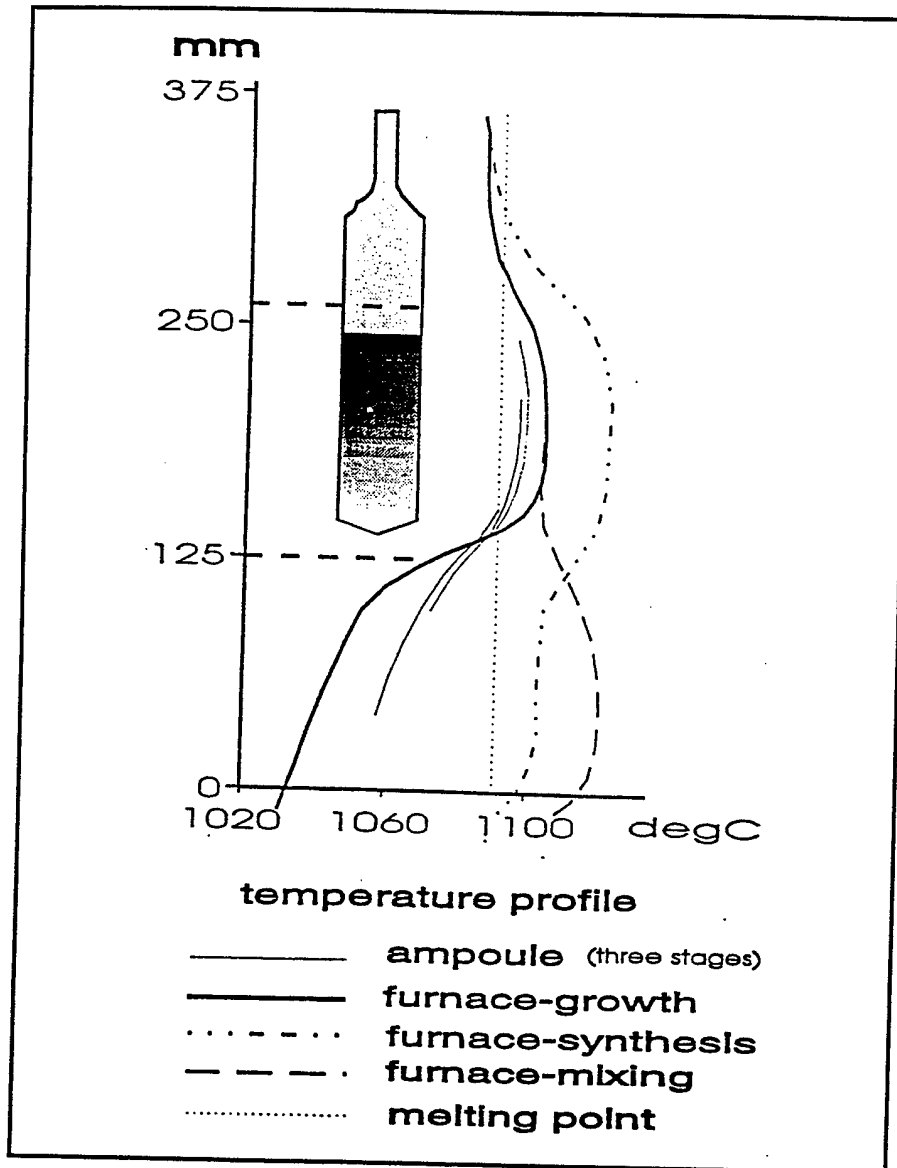


Figure 1 Schematic of experimental growth system.

3.4 Evaluation of Experimental Crystal Growth System

The crystals grown using this experimental system were characterized by excellent structural perfection as illustrated in Figure 2. This figure shows the crystalline boule and a cross section from a crystal of $\text{Cd}_{0.85}\text{Mn}_{0.15}\text{Te}:\text{V}$ (top) and $\text{Cd}_{0.55}\text{Mn}_{0.45}\text{Te}:\text{V}$ (bottom).

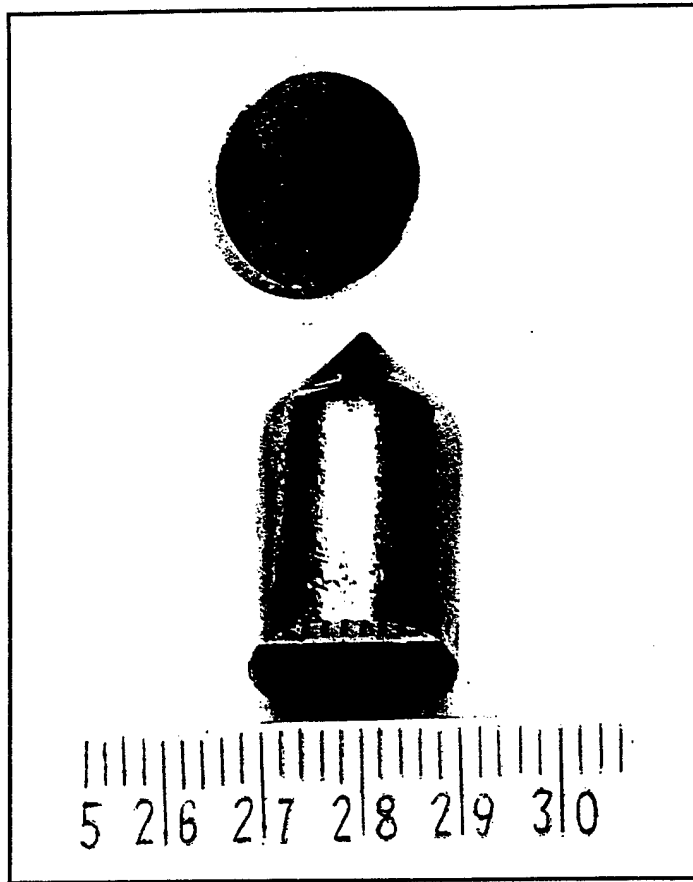


Figure 2 Photograph of $\text{Cd}_{0.85}\text{Mn}_{0.15}\text{Te}:\text{V}$

It was found both theoretically and experimentally that growth of $\text{Cd}_{1-x}\text{Mn}_x\text{Te}$ from the melt gives satisfactory results only in the Stockbarger configuration. In this system (which consists of two isothermal zones separated by a high gradient zone) the growth interface may be located in the hot zone, relatively far from the edge of the zone. The location of the growth interface and also its convex shape is controlled by the temperature of the hot zone and the cold zone.

The experimental problems that result from imposing optimal temperatures are because of the effects of the ampoule ends, especially for growth of large diameter or very short crystals [17-22]. Therefore initially, a very high difference between temperatures of the furnace zones was applied, with temperature of the hotter zone considerably exceeding the temperature of the melting point of the material. However, as shown in Figure 3, the best results for avoiding parasitic nucleation and minimizing thermal stress is a temperature profile with a high temperature zone that only slightly exceeds the temperature of the melting point [23]. In this case the short gradient zone can be used and a cold zone temperature only slightly lower than that of the hotter isothermal zone.

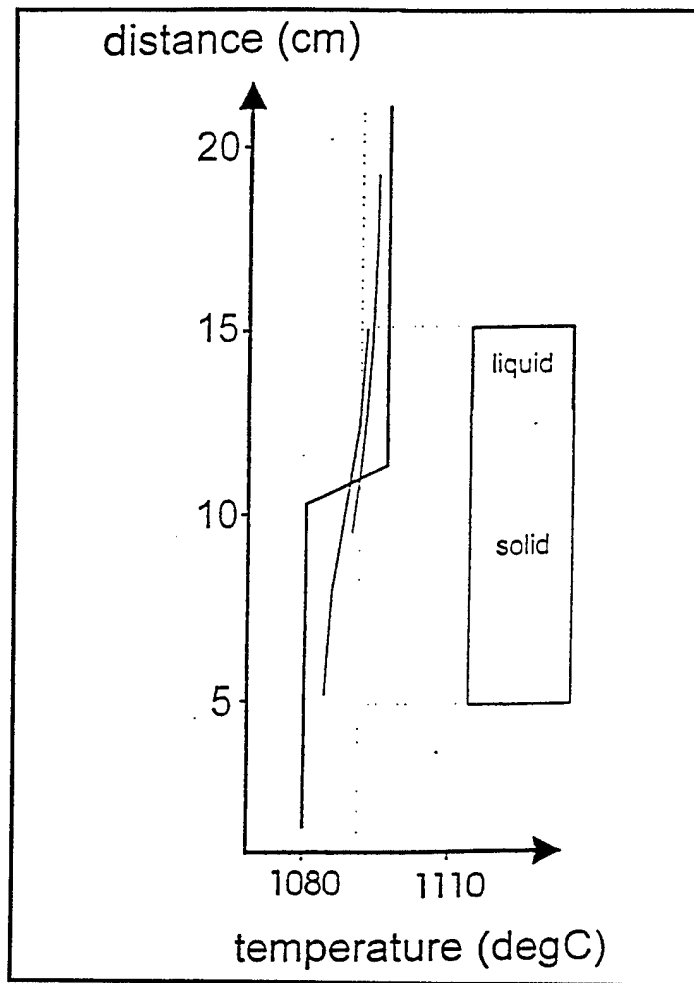


Figure 3 Temperature distribution computed along the axis of the charge/ampoule interface.

The difference of temperature between the isothermal zones depends on the difference between the temperature of the hotter zone and the melting point of the grown material. Therefore, minimizing one of these values will minimize the other, and hence, lead to a decrease in the radial temperature gradient and stress in the crystal.

Theoretically, crystals can be grown in two isothermal zones such that the crystal is slowly cooled following growth and maintained in the bottom zone under isothermal conditions. Practically, however, it is more convenient if the colder zone is not isothermal, but characterized by a linear temperature gradient. A linear temperature gradient introduces a higher longitudinal temperature gradient along the load and improves the stability of the interface [24].

The influence of a linear temperature gradient in the hot zone on growth conditions was also investigated. Compared to the former system, the only important effect that was observed was a more pronounced effect of the convex shape of the interface during the first stage of growth.

Conclusions resulting from our computational analysis and experiments can be summarized in two points:

1. From the point of view of minimizing radial temperature gradients and thermal stresses, the temperature of the cold zone should be kept as high as possible for growth of a convex interface. However, the difference between the temperature of the cold and hot zone is dependent on the difference between the temperature of the hot zone and the melting point. Both of these values must be lowered simultaneously.
2. In order to increase the axial temperature gradient (to improve stability and increase growth velocity without causing constitutional supercooling), a linear temperature gradient along the cold zone is mandatory. With such a temperature profile, growth of infinitely long low-stress crystals is possible.

Additionally it was confirmed, that the Stockbarger thermal configuration is superior to the parabola-like configuration of the Bridgman technique in the growth of single crystals of low thermal conductivity materials. The geometric and thermal parameters of the furnace should be chosen such that the lowest temperature gradient along the interface is high enough to avoid constitutional supercooling, and the heater temperature required to melt the charge is just enough above the melting point for the interface to be slightly convex.

The difference in construction of the real experimental furnace and the one used in computations had a minor effect on the quantitative results obtained from computations. The computations also gave a satisfactory description of the effects of changes in temperature and construction of the furnace on the quality of the obtained crystals. It can be concluded that the application of thermal baffles separating furnace zones has an effect on the temperature field similar to decreasing the diameter of the furnace.

4.0 Crystal Characterization

Several $\text{Cd}_{1-x}\text{Mn}_x\text{Te}$ crystalline boules were grown during this project. These crystals include:

vanadium doped with composition $x=0.15$ ($\text{Cd}_{0.85}\text{Mn}_{0.15}\text{Te}:\text{V}$);

vanadium doped with composition $x=0.45$ ($\text{Cd}_{0.55}\text{Mn}_{0.45}\text{Te}:\text{V}$);

chromium doped with composition $x=0.15$ ($\text{Cd}_{0.85}\text{Mn}_{0.15}\text{Te}:\text{Cr}$);

undoped with composition $x=0.15$ ($\text{Cd}_{0.85}\text{Mn}_{0.15}\text{Te}$); and

undoped with composition $x=0.45$ ($\text{Cd}_{0.55}\text{Mn}_{0.45}\text{Te}$).

Samples from each of these boules were prepared in the shape of traditional wafers as well as cubes. The cubes were approximately $5 \times 5 \times 5 \text{mm}^3$ with $[110] \times [110] \times [100]$ orientations, and the wafers were cut along the $[110]$ direction. The wafers and cubes were mechanically lapped and polished to an optical finish.

Several techniques were used to characterize the $\text{Cd}_{1-x}\text{Mn}_x\text{Te}$ crystals. These characterization techniques included: electrical measurements, absorption and emission spectroscopy, photoluminescence, magneto-optic measurements, infrared microscopy, and photorefractivity.

4.1 Electrical Measurements

$\text{Cd}_{1-x}\text{Mn}_x\text{Te}$ typically exhibits very high resistance. As a result, it is difficult to measure the electrical properties for such crystals because of non-ideal conditions such as leakage current or contact problems. Further complications arise from limitations of the measuring instruments. Hall measurements using the Van der Pauw technique can not be performed in very high resistivity samples since small input currents produce voltages beyond the capability of the measuring equipment. An alternative method to measure the resistivity uses a simple circuit in which the sample is connected in series with known and thermally stable resistors. Measurement of the applied voltage and the voltage drop across the resistor determines the current in the circuit. The resistivity can then be calculated from the series current and the voltage drop across the sample. Regardless of the method used to determine the resistivity, measurements were taken over a range of values to verify that the contacts were ohmic.

The high resistivity of $\text{Cd}_{1-x}\text{Mn}_x\text{Te}$ material also makes it difficult to form low resistance ohmic contacts to the crystals. For this study, contacts were formed by ion cleaning the surface of the crystals and depositing gold onto the cleaned surface. The linear relationship between current and voltage seen in a highly resistive $\text{Cd}_{0.55}\text{Mn}_{0.45}\text{Te}:\text{V}$ crystal is shown in figure 4. These contacts displayed low resistance ohmic conductivity and the electrical properties of the crystals were successfully measured.

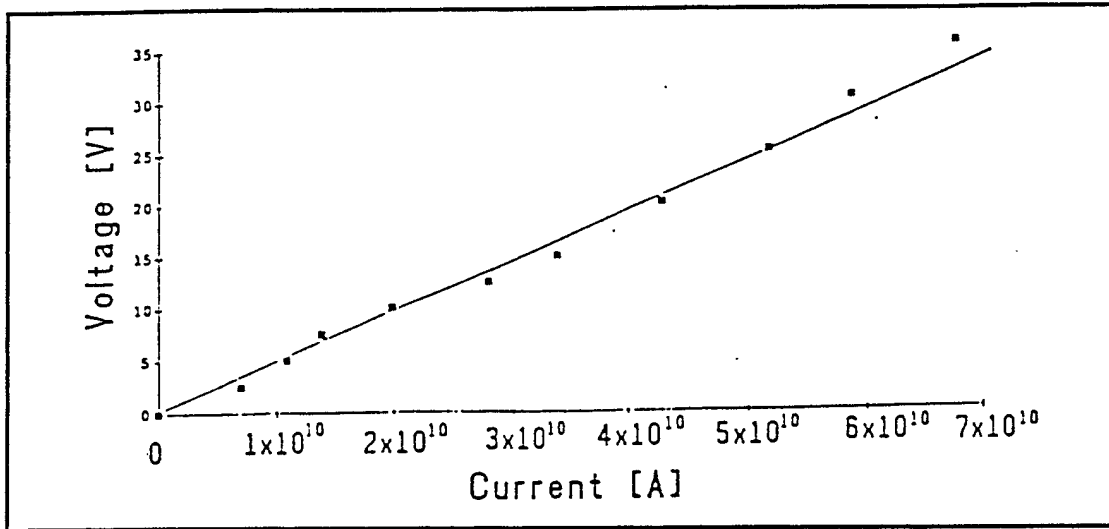


Figure 4 I-V characteristics for $\text{Cd}_{0.55}\text{Mn}_{0.45}\text{Te}:\text{V}$.

Initially, measurements were taken under dark conditions so that photogenerated carriers were negligible. Measurements were also taken when the crystals were illuminated with laser radiation. $\text{Cd}_{0.55}\text{Mn}_{0.45}\text{Te}:\text{V}$ was studied using a tunable titanium sapphire laser at wavelengths of 1 micron and 750nm. The measured values of resistivity for this crystal were found to be: 2.3×10^{10} ohm-cm under dark conditions, 1.0×10^8 ohm-cm under $\lambda=1$ micron radiation, and 7.7×10^6 ohm-cm under $\lambda=0.750$ microns. This crystal showed a change in resistivity of almost four orders of magnitude between dark conditions and illumination with radiation of 750nm wavelength.

A plot of current versus voltage for a sample of $\text{Cd}_{0.85}\text{Mn}_{0.15}\text{Te}$ is shown in figure 5. This sample displayed an approximately 15% reduction in conductivity when the fluorescent room lights were turned off, thus exhibiting fairly high photoconductivity.

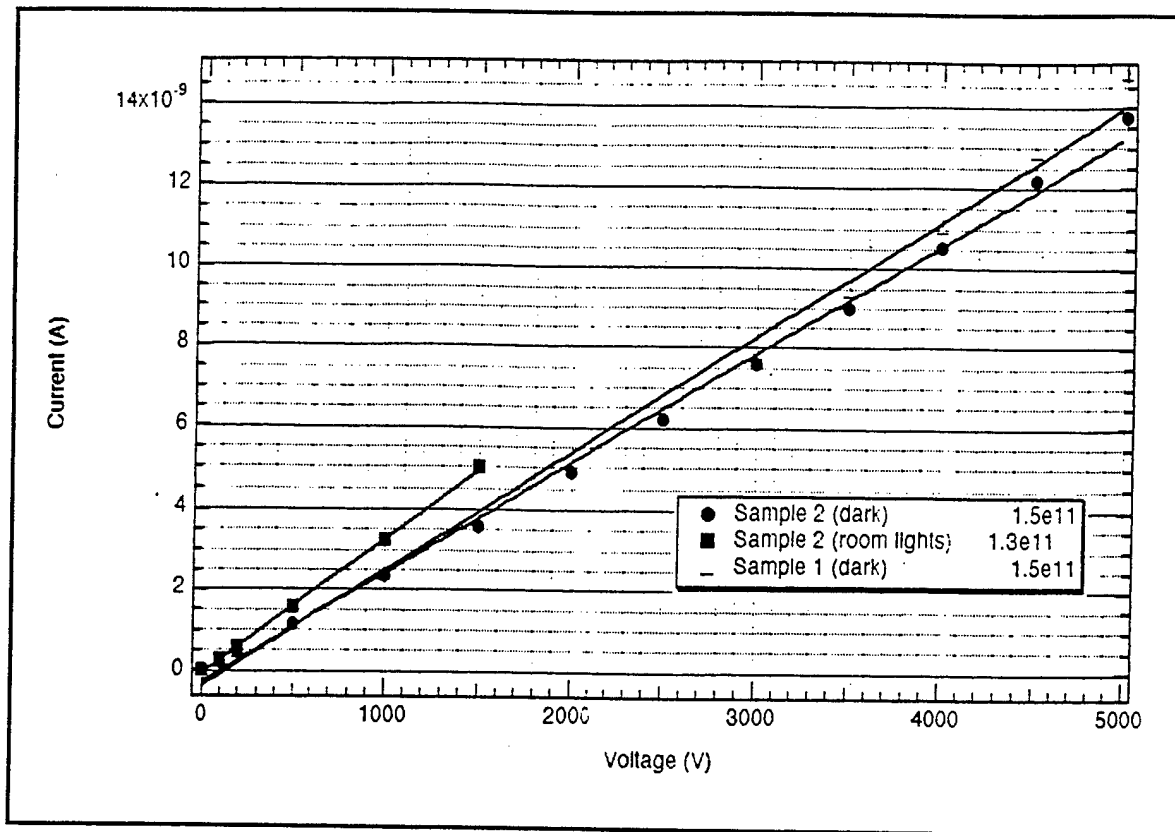


Figure 5 Conductivity of $\text{Cd}_{0.85}\text{Mn}_{0.15}\text{Te}:\text{V}$

The undoped $\text{Cd}_{0.55}\text{Mn}_{0.45}\text{Te}$ crystals displayed lower resistivity and Van der Pauw measurements were possible. These crystals were studied using a helium-neon laser with wavelength 632.8nm. The results showed a Hall coefficient of 1.5×10^8 , a hole mobility of $83 \text{ cm}^2/\text{Vs}$, and a hole concentration of $4.2 \times 10^{10} \text{ cm}^{-3}$.

4.2 Magneto-optic and Absorption Measurements:

The magneto-optic and absorption measurements of both undoped and vanadium doped $\text{Cd}_{0.55}\text{Mn}_{0.45}\text{Te}$ crystals were investigated. The key parameters characterizing a magneto-optical material are the attenuation, α , and the Verdet constant, V . The Verdet constant is defined as the amount of rotation of polarization per unit length per unit magnetic field:

$$V = q/(lB) [^\circ/\text{cmG}]$$

where q is the amount of rotation, l is the thickness of the crystal and B is the magnetic field. V is a function of photon energy, temperature and the magnetic properties of the crystal. For the design of devices employing the magneto-optic properties of a material, a large Verdet constant is desirable.

Unfortunately, materials with large values of Verdet constant usually have large attenuation which results in large insertion losses [25]. Therefore, the figure of merit, defined as F , is used as a comparative value for magneto-optical materials where

$$F = V / a \text{ [}^\circ\text{/dB Gauss]}$$

and a is the attenuation expressed in dB/cm.

The experimental configuration used to measure the rotation of polarization in the CdMnTe crystals is pictured in figure 6. A helium-neon (He-Ne) laser was used to provide a collimated optical beam at a wavelength of 0.6328 microns, and a 1 kGauss permanent magnet provided a steady magnetic field. The CdMnTe crystal was placed between the plates of the magnet and small mirrors were used to direct the laser light through the crystal in a direction parallel to the magnetic field. The Faraday rotation was determined by the use of two polarizing films. The first film was stationary and served to polarize the light incident on the sample. Once the light was transmitted through the sample, a second polarizer analyzes the rotated polarization. The polarizers were originally set normal to each other so that no light passed into the detector. When the crystal was placed in the magnetic field, the polarization of the light rotated as it propagated through the material. The second polarizer was then rotated to the null position. In this way, the rotation of the polarization of the light was determined by the amount of rotation of the second polarizer.

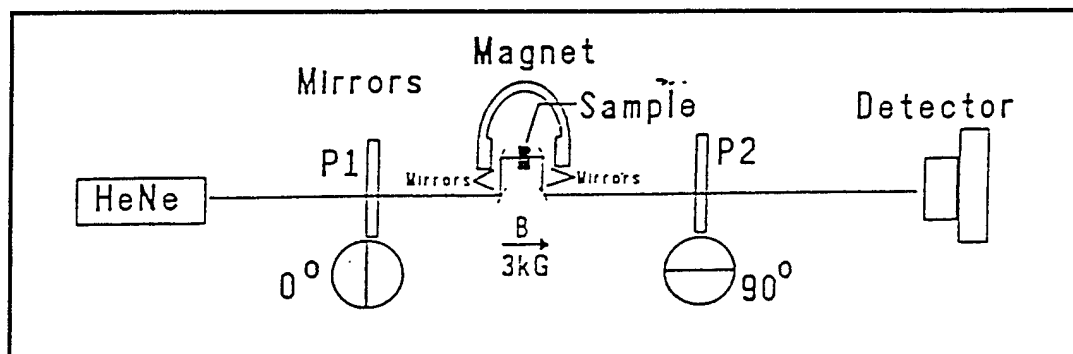


Figure 6 Apparatus used to measure polarization rotation.

The absorbance of the $\text{Cd}_{0.55}\text{Mn}_{0.45}\text{Te}$ crystals was measured using a Perkin-Elmer Model 330 dual-beam UV-Visible spectrophotometer. Output was plotted as absorbance (A) versus wavelength (λ). The absorption coefficient versus wavelength was determined from the absorbance according to

$$a = 2.303 A / l \text{ [cm}^{-1}\text{]}$$

where l is the optical path length through the crystal in centimeters. The attenuation at each wavelength was also expressed in terms of loss in decibels per centimeter (dB/cm) through the expression

$$\text{loss} = 10 A / l \text{ [dB/cm]}.$$

The spectra obtained using the UV-visible spectrometer for two undoped $\text{Cd}_{0.55}\text{Mn}_{0.45}\text{Te}$ crystals, expressed as absorption coefficient versus wavelength, is shown in figure 7. These measurements, however, do not consider losses due to reflection at the surface of incidence. As a result, the correct absorption of the material is less than the values obtained from the UV-visible spectrometer. The insertion loss of a device can be reduced to the intrinsic absorption loss of the material with the use of anti-reflective coatings. Therefore, a calculated value for the absorption of the $\text{Cd}_{0.55}\text{Mn}_{0.45}\text{Te}$ crystals at 632.8nm was determined from experimental measurements of reflection coefficient.

The absorption properties of $\text{Cd}_{0.55}\text{Mn}_{0.45}\text{Te}:\text{V}$ were measured using the ratio of the power of the transmitted and incident beams of a helium-neon laser ($\lambda=632.8\text{nm}$). The loss resulting from reflection was taken into account in these measurements.

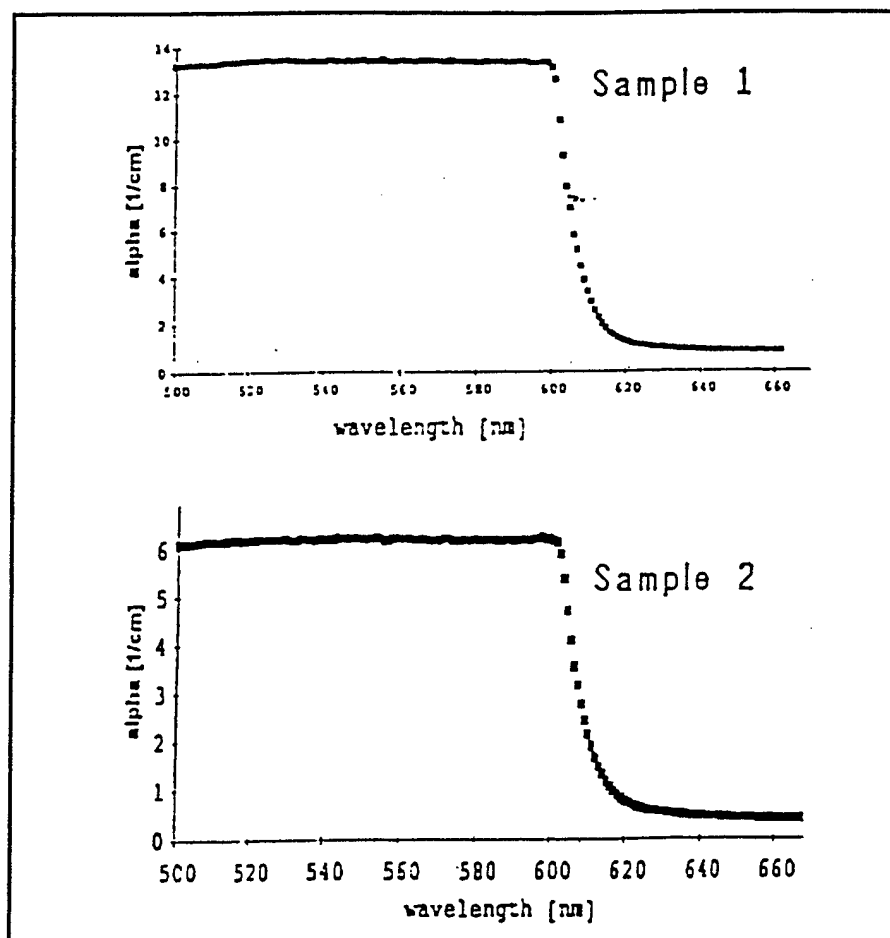


Figure 7 Absorption coefficient versus wavelength for $\text{Cd}_{0.55}\text{Mn}_{0.45}\text{Te}$.

The calculated values of attenuation and magneto-optic parameters at $\lambda = 632.8\text{nm}$ for 2 samples of $\text{Cd}_{0.55}\text{Mn}_{0.45}\text{Te}$, an as-grown sample of $\text{Cd}_{0.55}\text{Mn}_{0.45}\text{Te}:\text{V}$ and an annealed sample of $\text{Cd}_{0.55}\text{Mn}_{0.45}\text{Te}:\text{V}$ are listed in Table 1.

These results clearly show that $\text{Cd}_{0.55}\text{Mn}_{0.45}\text{Te}$ is a suitable material for high quality magneto-optic device applications, with properties far superior to those of previously reported materials used in magneto-optic applications at wavelengths less than 1 micron. These results also show that the vanadium doped crystals exhibit magneto-optic behavior as well.

		x=0.45 (1)	x=0.45 (2)	V doped (ag)	V doped (Ann)	units
Absorbance	A	.003	0.003	1.23	0.803	
Attenuation	a	0.17	0.08	31.1	22.9	dB/cm
Absorption Coefficient	a	0.04	0.017			cm ⁻¹
Verdet Constant	V	0.052	0.062	0.082	0.072	°/cmG
F (V/a)		0.70	0.80	0.0026	0.0031	°/dBG

Table I The calculated values of attenuation and magneto-optic parameters at $\lambda = 632.8\text{nm}$ for 2 samples of $\text{Cd}_{0.55}\text{Mn}_{0.45}\text{Te}$, an as-grown sample of $\text{Cd}_{0.55}\text{Mn}_{0.45}\text{Te}:\text{V}$ and an annealed sample of $\text{Cd}_{0.55}\text{Mn}_{0.45}\text{Te}:\text{V}$.

4.3 Photoluminescence Measurements

The photoluminescence spectrums for $\text{Cd}_{0.55}\text{Mn}_{0.45}\text{Te}$ and $\text{Cd}_{0.55}\text{Mn}_{0.45}\text{Te}:\text{V}$ are shown in figures 8 and 9. The spectrum from each crystal displayed the most intense luminescence peak at approximately 2.01eV. This peak corresponds to the transitions within the localized states of the Mn^{2+} ions. These results indicate that this transition occurs at approximately 2.01 to 2.02 eV in $\text{Cd}_{0.55}\text{Mn}_{0.45}\text{Te}$ at 4K. This peak is also very prominent in $\text{Cd}_{0.55}\text{Mn}_{0.45}\text{Te}:\text{V}$ indicating that the energy difference between the ground level and the first excited state of manganese is not affected by the presence of vanadium.

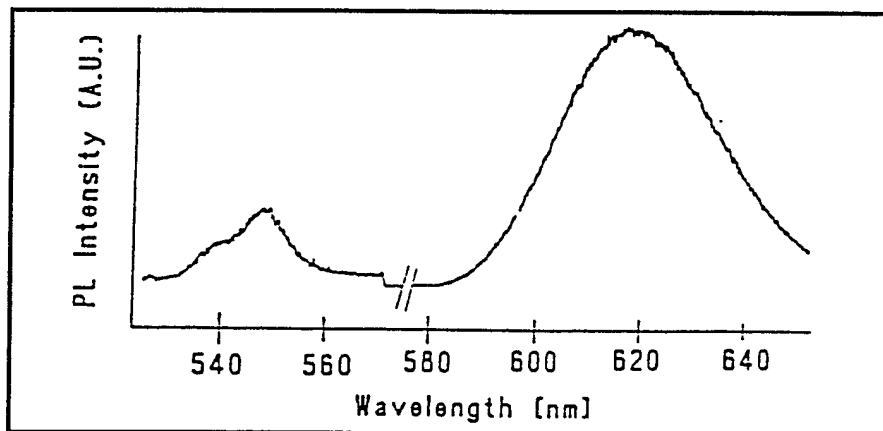


Figure 8 Photoluminescence spectrum of $\text{Cd}_{0.55}\text{Mn}_{0.45}\text{Te}$.

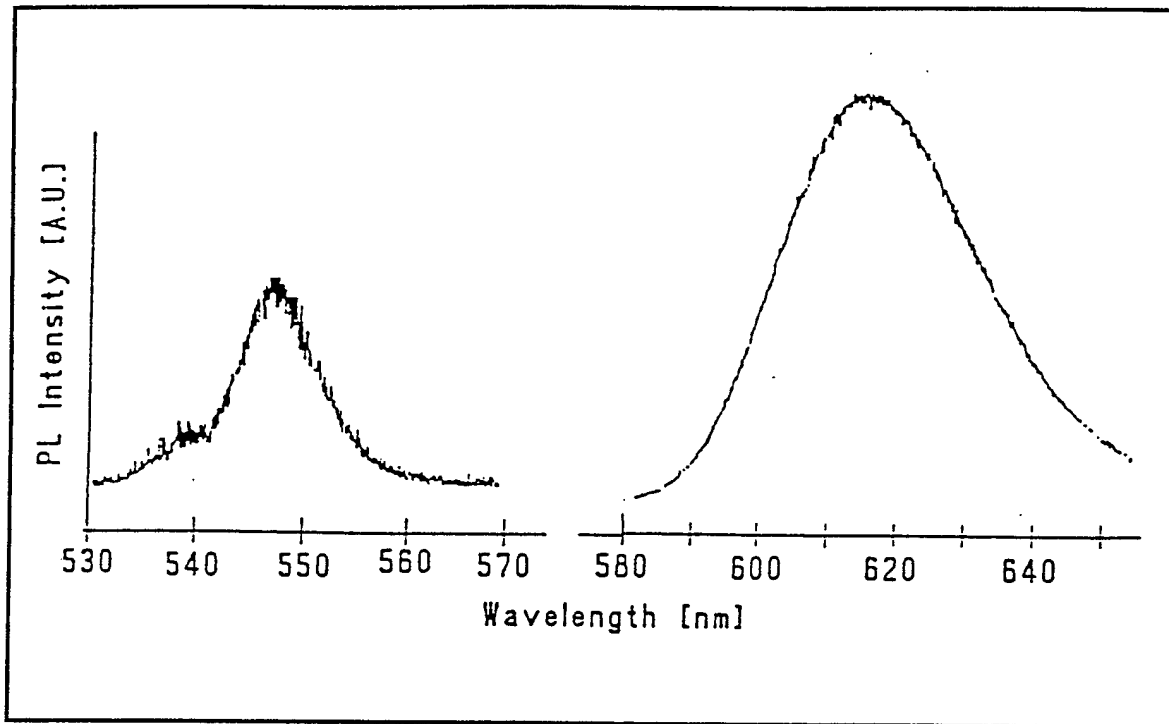


Figure 9 Photoluminescence spectrum of Cd_{0.55}Mn_{0.45}Te:V.

The other luminescence peaks for these samples were far less intense than the one at 2.01eV. The undoped and vanadium doped Cd_{0.55}Mn_{0.45}Te crystals displayed luminescence at 2.27eV with a small shoulder on the high energy side of this peak at approximately 2.3eV. These peaks were less than one-tenth of the intensity of the peak at 2.0eV. We believe that these luminescence peaks are a result of transitions between the valence band and conduction band in Cd_{0.55}Mn_{0.45}Te corresponding to an energy band gap of approximately 2.27eV. This value is in agreement with previously reported values for this material of $E_{\text{gap}} \approx 2.29 \text{ eV}$.

For Cd_{0.55}Mn_{0.45}Te:V and Cd_{0.55}Mn_{0.45}Te, luminescence at approximately 2.30 eV appears as a small shoulder on the 2.27eV peak. We believe that this peak is composition independent based on earlier measurements and is most likely an intrinsic characteristic of the CdMnTe system.

This luminescence may be a result of interactions between the manganese ions and the band electrons, or a result of energy levels associated with native defects in the CdMnTe lattice. The former explanation is not likely since the large energies needed to change Mn²⁺ to the Mn³⁺ or Mn⁺ configurations make it difficult for Mn to exchange electrons with the band states. Therefore, it is believed that this peak is caused by native defects. The primary native defect in CdTe was determined to be cadmium vacancies, which are assumed to act as double acceptors [26,27].

Further investigation into the effect of native defects on the energy band structure of CdMnTe is necessary to confirm the transition responsible for the photoluminescence peak at 2.3 eV.

4.4 Absorption and Emission Measurements:

The absorption and emission spectra of chromium doped $\text{Cd}_{0.85}\text{Mn}_{0.15}\text{Te}$ were measured. Figure 10 shows a plot of the absorbance versus wavelength of the crystal for wavelengths from 900nm to 2500nm. A strong absorption line corresponding to the chromium ion (Cr^{2+}) is present. This peak indicates that this material has the potential for being a solid state material with lasing wavelength around 1.9 microns. The absorption spectrum also indicates that there are two ranges of wavelength over which the crystal may display photorefractive properties: those wavelengths around 1000nm and those around 1500nm.

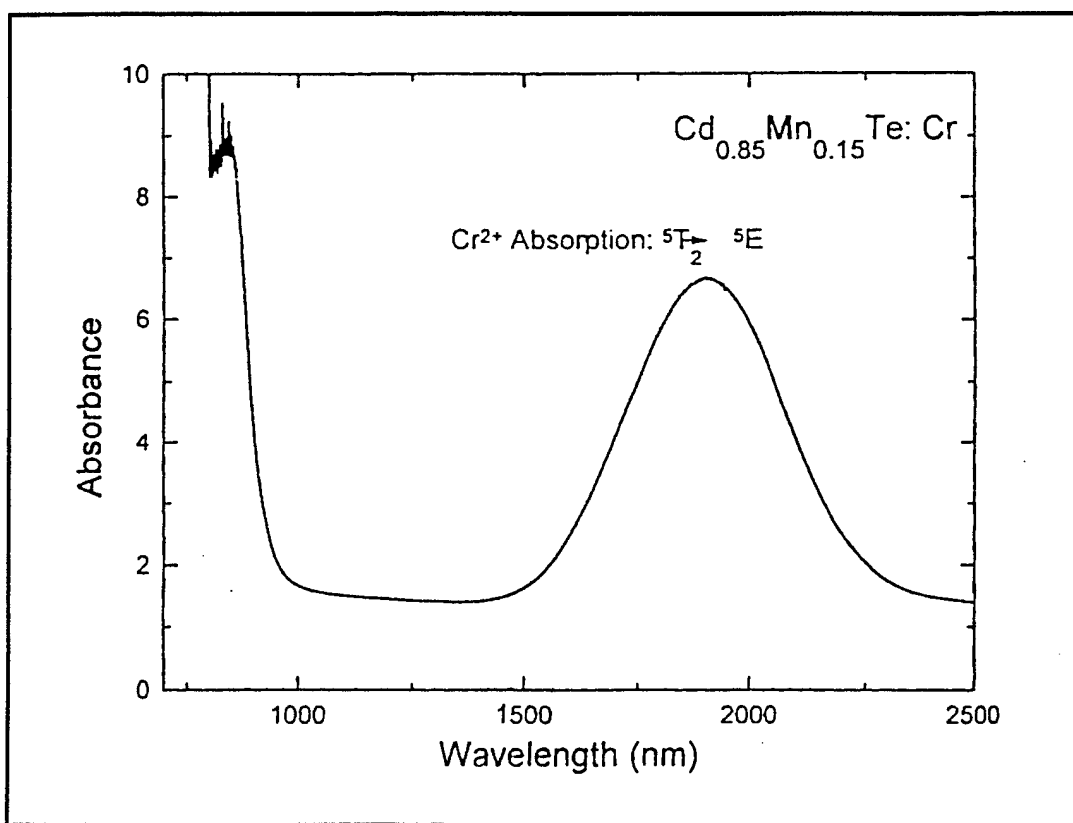


Figure 10 Absorption spectrum of $\text{Cd}_{0.85}\text{Mn}_{0.15}\text{Te}:\text{Cr}$.

Figure 11 shows a plot of emitted intensity versus wavelength for a sample excited with radiation from an argon ion laser (488nm) at temperatures of 15K, 100K, 200K and 300K.

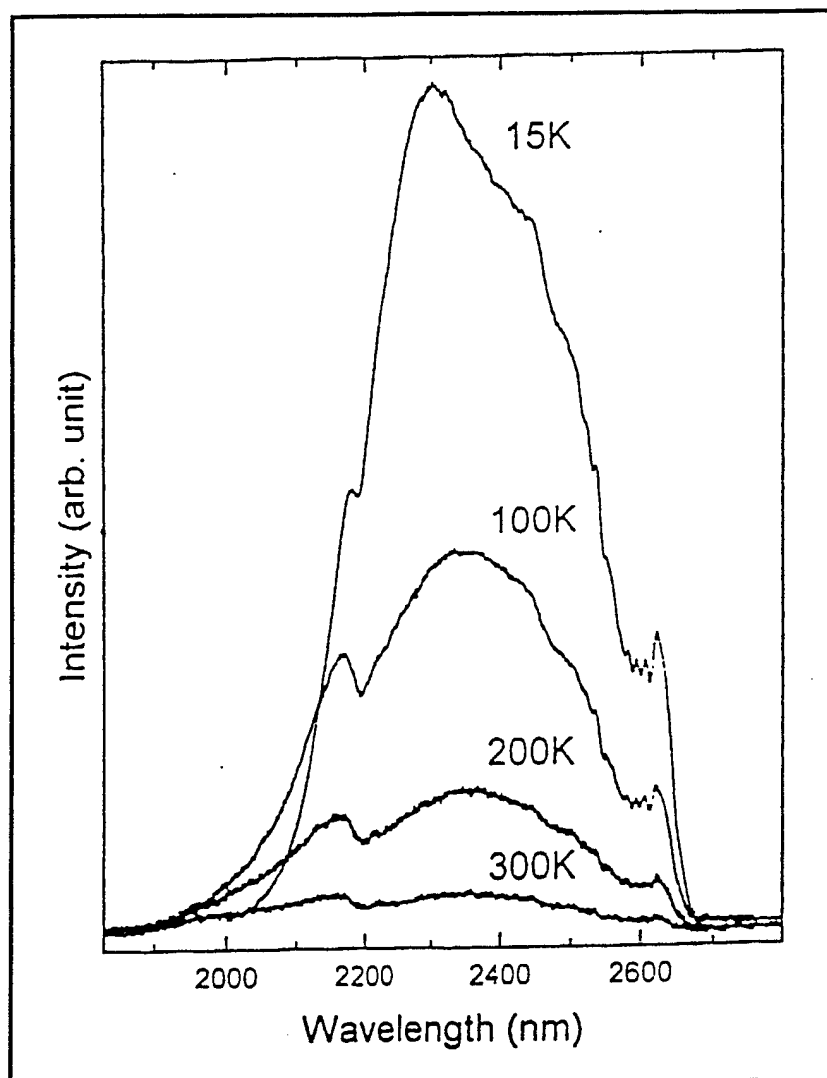


Figure 11 Emission spectrum of $\text{Cd}_{0.85}\text{Mn}_{0.15}\text{Te}:\text{Cr}$ at various temperatures using an argon ion laser (488nm) as the excitation source.

Figure 12 shows a similar plot of emitted intensity versus wavelength at various temperatures using a 790nm diode laser as the excitation source. This laser was significantly stronger (more than a factor of 20) than the argon ion laser used previously.

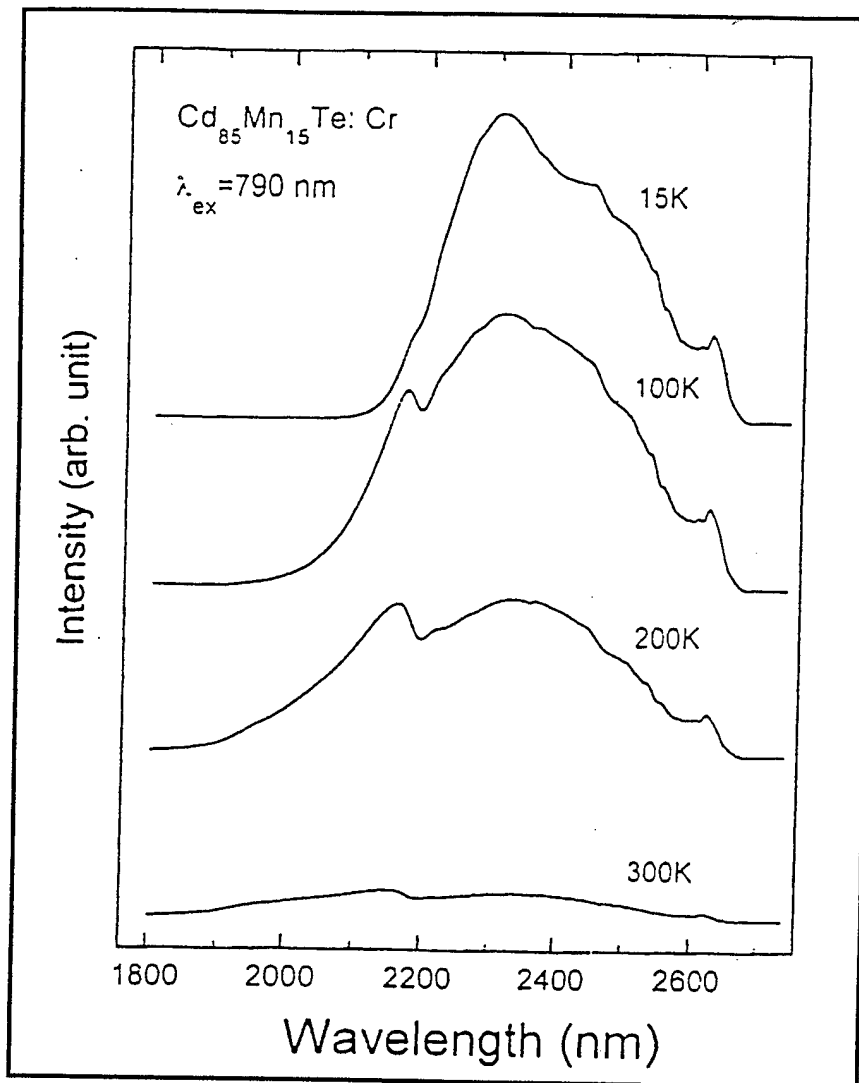


Figure 12 Emission spectrum of $\text{Cd}_{0.85}\text{Mn}_{0.15}\text{Te}:\text{Cr}$ at various temperatures using a 790nm diode laser as the excitation source.

Finally, figure 13 displays the integrated emitted intensity versus temperature for both excitation sources. We found that the temperature dependence of the integrated emission is different for 790nm and 488nm excitations.

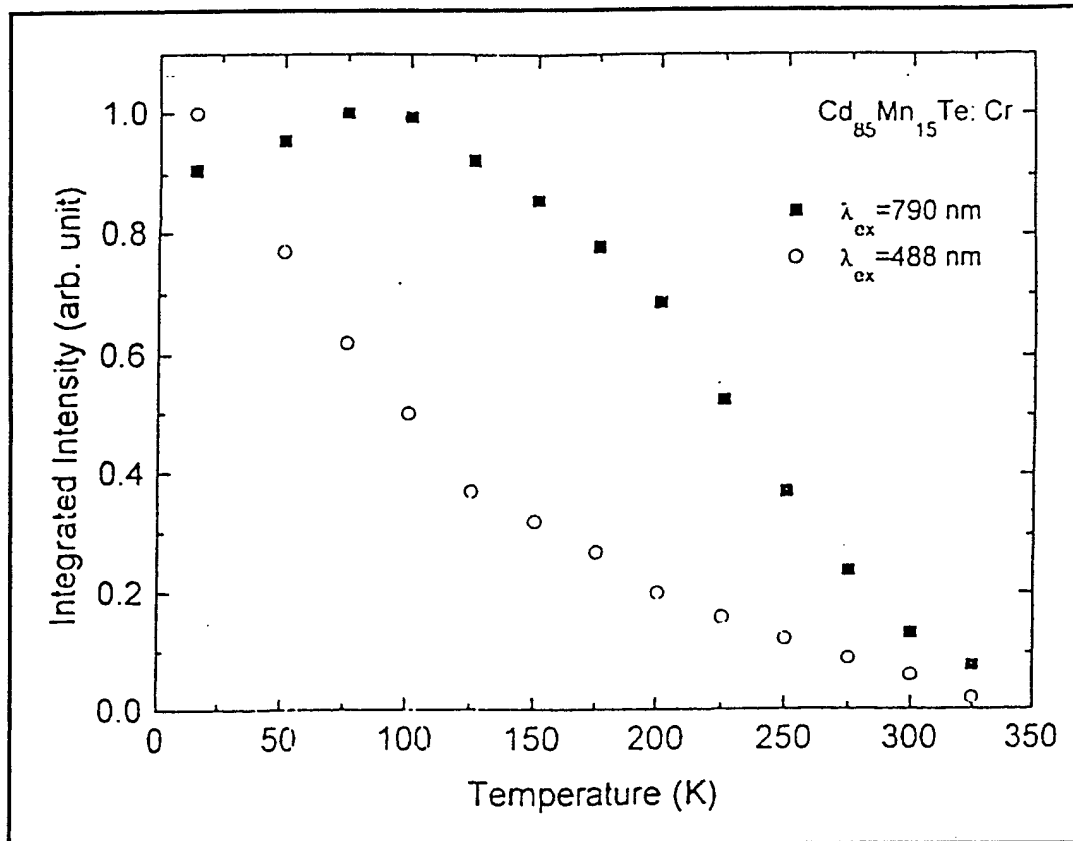


Figure 13 Integrated emission intensity versus temperature for $\text{Cd}_{0.85}\text{Mn}_{0.15}\text{Te}:\text{Cr}$.

4.5 Infrared Microscopy

Using the transmission mode of a high powered visible/infrared microscope, details within the bulk structure of the $\text{Cd}_{1-x}\text{Mn}_x\text{Te}$ crystals were observed. Figure 14 is a photograph taken using this microscope within the bulk of a $\text{Cd}_{0.55}\text{Mn}_{0.45}\text{Te}:\text{V}$ crystal. The small spots in the photo on the left represent possible voids that were located at one plane within the bulk of the crystal. The dark areas in the photo on the right represent possible precipitates.

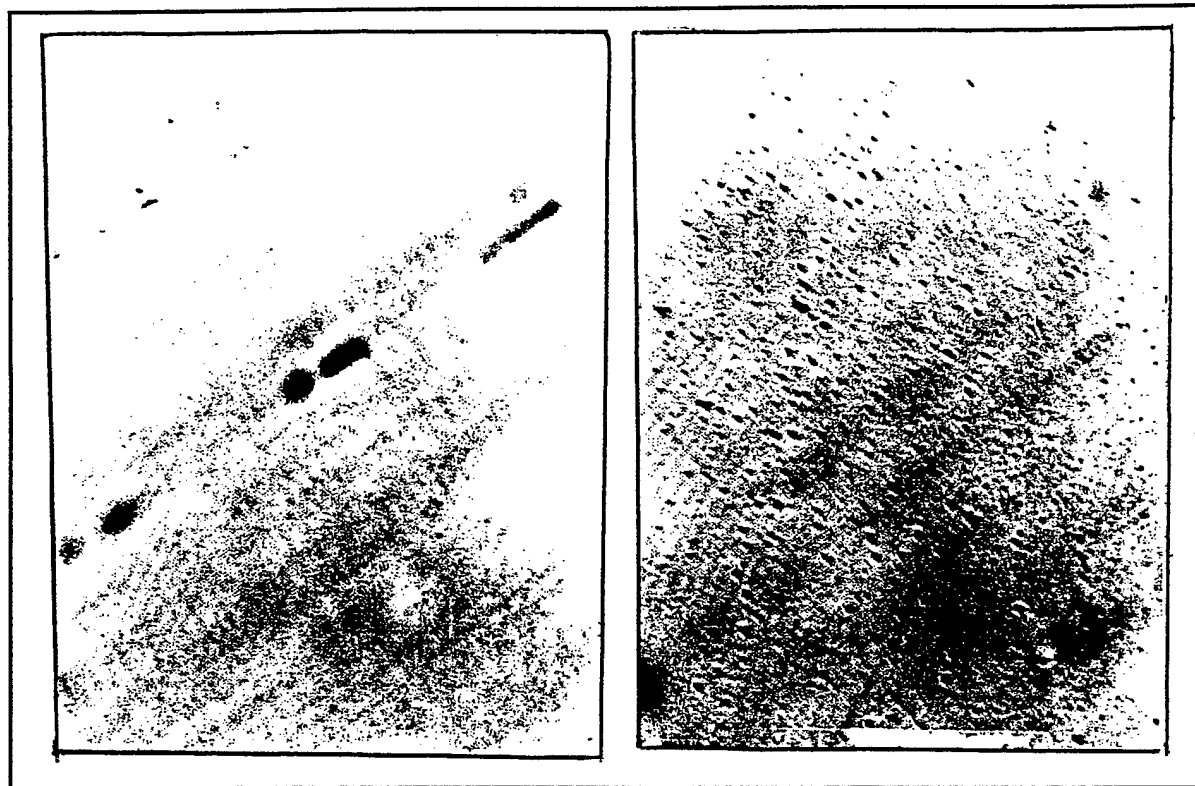


Figure 14 IR microscope picture of Cd_{0.55}Mn_{0.45}Te:V.

Figure 15 is a similar photograph for a sample of Cd_{0.85}Mn_{0.15}Te:V. The photo on the left shows the presence of decorated twins (clusters of impurities on the borders of the twins) within the bulk of the crystal. The right photo also shows the presence of precipitates within the bulk.

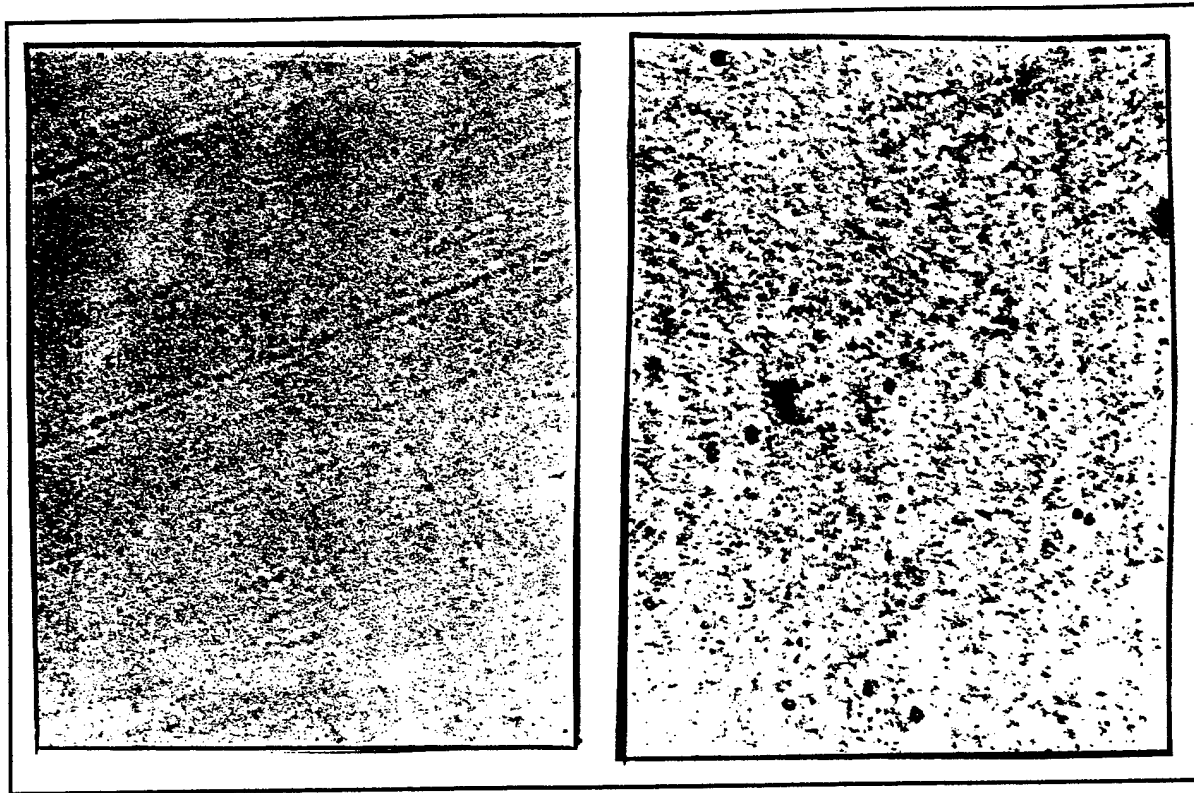


Figure 15 IR microscope picture of $\text{Cd}_{0.85}\text{Mn}_{0.15}\text{Te}:\text{V}$.

During this project, we also used infrared microscopic techniques to examine the crystal structure of the as-grown and annealed $\text{Cd}_{0.40}\text{Mn}_{0.60}\text{Te}:\text{V}$ crystals. Dark traces were clearly apparent in this crystal. These dark areas are considered to be tellurium precipitates which act as optical scattering centers in the bulk of the crystal. These precipitates range in size from approximately $12 \times 12 \text{mm}^2$ to $25 \times 25 \text{mm}^2$. On average, the concentration of precipitates was approximately $630/\text{mm}^2$.

The photographs shown in figure 16 are for a $\text{Cd}_{0.40}\text{Mn}_{0.60}\text{Te}:\text{V}$ crystal after a 24 hour, 900°C annealing treatment in an atmosphere of excess cadmium. The concentration of tellurium precipitates in the annealed crystal is dramatically reduced, and those that remain are extremely small. During the annealing procedure, it is believed that the excess tellurium diffuses to the surface of the crystal, and therefore is removed during polishing.

From this study, we have found that high temperature annealing of $\text{Cd}_{1-x}\text{Mn}_x\text{Te}$ can have a profound effect on the use of this material in devices. Prior to annealing, the high absorption of the $\text{Cd}_{0.40}\text{Mn}_{0.60}\text{Te}$ crystal precludes its use in many optical applications. After annealing, however, the absorption is greatly reduced, making $\text{Cd}_{0.40}\text{Mn}_{0.60}\text{Te}$ a suitable material for several device applications.

Therefore, post-growth annealing can be used to improve the properties of $\text{Cd}_{1-x}\text{Mn}_x\text{Te}$ and greatly enhance its usefulness in optical and electro-optic applications.

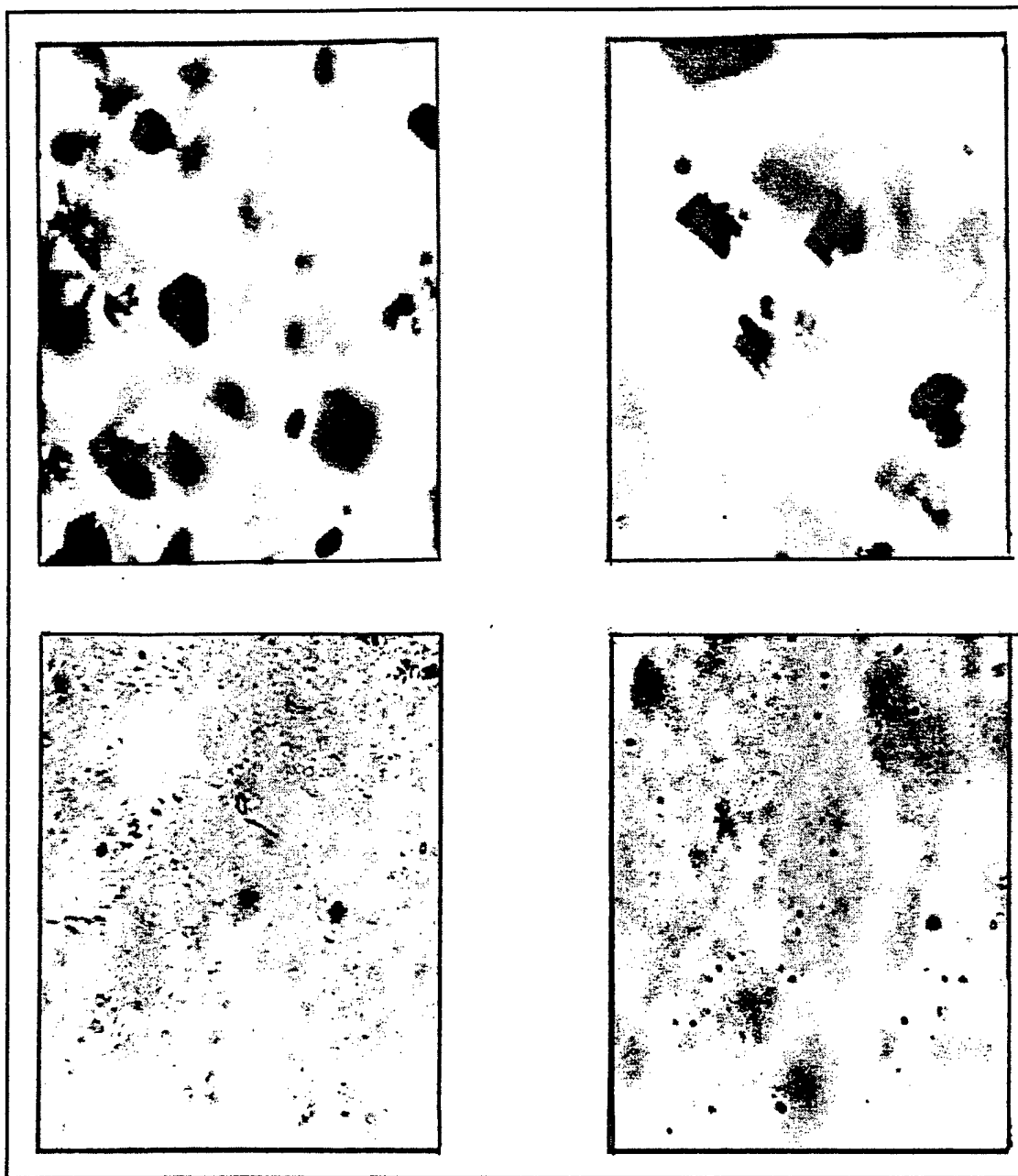


Figure 16 IR microscope pictures of as-grown (top) and annealed (bottom) $\text{Cd}_{0.40}\text{Mn}_{0.60}\text{Te}$.

4.6 Photorefractive Characterization

Transmission spectrum, two beam coupling gain coefficient and grating time constant for $\text{Cd}_{0.55}\text{Mn}_{0.45}\text{Te}:\text{V}$ were investigated. Photorefractive two-beam coupling was observed from 0.63 to 1.3mm. The photorefractive gain under diffusion conditions at 0.75mm and a 1mm grating period was 0.4cm^{-1} and the effective trap concentration was calculated to be about $1.2 \times 10^{15}\text{cm}^{-3}$. The absorption coefficient at 0.75mm was 2.3cm^{-1} . A photorefractive gain as high as 5.6cm^{-1} at 15mm grating period with square wave ac fields of 7kV/cm was observed.

The value of the electro-optic coefficient at 0.75mm was derived using the fit of the two-beam mixing data at 0.75mm, where single charge carrier and a single trap model was assumed. The value of the electro-optic coefficient was also directly measured at 0.75mm by measuring the electro-optic retardation of a weak probe beam. This value was measured to be 2.8 pm/V which is close to the value that was derived from the two-wave mixing measurements. This value suggests that the electron-hole competition coefficient is not significant at this wavelength. We did observe, however, the presence of electron-hole competition in the photorefractive $\text{Cd}_{0.85}\text{Mn}_{0.15}\text{Te}:\text{V}$ crystals. In the samples prepared from this crystal, photorefractivity was observed from 0.75 to 1.5mm. The sign of the photorefractive gain reversed polarity at a wavelength of approximately 1.06mm. This was the first time that we observed electron-hole competition in crystals prepared at Brimrose.

5.0 Conclusions and Possible Future Work

During this project, we have grown several $\text{Cd}_{1-x}\text{Mn}_x\text{Te}:\text{V}$ crystals that displayed photorefractive behavior. The results of the characterization of these crystals attest to the degree of crystalline quality that was obtained. However, there are still many possible avenues for further improvement that should be explored.

One possibility for improving the photorefractive gain and overall crystalline quality of $\text{Cd}_{1-x}\text{Mn}_x\text{Te}:\text{V}$ is to investigate the use of solution growth. In crystal growth from solution, a saturated solution of CdMnTe in a solvent of tellurium is used. Growth occurs after the solution of the material is supersaturated either by evaporating the solvent (isothermally) or by lowering the solution temperature (non-isothermally). For growth of high quality $\text{Cd}_{1-x}\text{Mn}_x\text{Te}:\text{V}$, we would investigate the use of the travelling heater method (THM). THM provides the advantages of: crystal growth at low temperatures; better compositional homogeneity, lower defect density and less limitations in diameter and length of the crystal.

The use of post growth annealing should also be investigated further as a method to improve the crystal quality of $\text{Cd}_{1-x}\text{Mn}_x\text{Te}:\text{V}$. The effect of annealing is dictated by the pressure-temperature phase diagram at a specific composition. Therefore, detailed analysis of the effect of thermal annealing at various temperatures must be investigated in order to optimize material parameters.

6.0 References

- [1] A. Partovi, J. Millerd, E.M. Garmire, M. Ziari, W.H. Steier, S.B. Trivedi and M.B. Klein. *Appl. Phys. Lett.* **57**, 846 (1990).
- [2] M. Ziari, W.H. Steier, P.N. Ranon, M.B. Klein and S.B. Trivedi. *J. Opt. Soc. Am. B.* 1461-1466 (1992).
- [3] R.N. Schwartz, M. Ziari and S.B. Trivedi. *Phys. Rev. B*, **49**, 5274 (1994).
- [4] M. Ziari, W.H. Steier, P.N. Ranon, M.B. Klein and S.B. Trivedi. paper presented at the *Annual Meeting of the Optical Society of America*, Nov. 3-8, 1991, San Jose, CA.
- [5] M. Ziari, W.H. Steier, P.N. Ranon, M.B. Klein and S.B. Trivedi. *Appl. Phys. Lett.* **60**, 1052 (1992).
- [6] M. Ziari, W.H. Steier, P.N. Ranon, M.B. Klein and S.B. Trivedi. Paper presented at the *Topical Meeting on Photorefractive Materials, Effects and Devices*, July 29-31, 1991, Beverl MA.
- [7] G.A. Brost, K.M. Madge, and S.B. Trivedi paper presented at the *MRS 1994 Spring Meeting*. also to be published in *Optical Materials*.
- [8] S.B. Trivedi, R.D. Rosemeier, G.A. Brost, K.M.Madge, and J.J. Kennedy. Paper presented at *ACCG/East-94 Conference*, Oct. 4-7 1994.
- [9] L. Kowalczyk. *J. Crys. Growth* **72**, 389 (1985).
- [10] C.E. Huang, D. Elwell and R. S. Feigelson, *J.Crystal Growth* **69** (1984) 274.
- [11] C. Parfeniuk, F. Weinberg, I. V. Samarasekera, C. Schvezov and L. Li, *J.Crystal Growth* **119** (1992) 261.
- [12] R. Siegel and J.R. Howel, "Thermal Radiation Heat Transfer" (*McGraw-Hill*, New York 1972).
- [13] K. Graszka and U. Zuzga-Graszka, *J. Crystal Growth* **116** (1992) 139.

- [14] Ch. Steer, M. Hage-Ali, P. Siffert, Mathematical Model for the Simulation of Crystallization of CdTe in a Vertical Bridgman Furnace, in: ed. R.B. James, *MRS Symposium Proceedings* 302 (1993).
- [15] W. Giriat and J. Furdyna. *Semiconductors and Semimetals*, Vol. 25, eds. R. K. Willardson and A. C. Beer. Academic, New York, 1988.
- [16] C.E. Chang and W.R. Wilcox, *J.Crystal Growth* **21** (1974) 135.
- [17] T.I. Ejim, W.A. Jesser and A.L. Fripp, *J.Crystal Growth* **69** (1984) 509.
- [18] T.W. Clyne, *J.Crystal Growth* **50** (1980) 684.
- [19] T.W. Clyne, *J.Crystal Growth* **50** (1980) 691.
- [20] C.L. Jones, P. Capper and J.J. Gosney, *J. Crystal Growth* **56** (1982) 581.
- [21] C.L. Jones, P. Capper J.J. Gosney and I. Kenworthy, *J.Crystal Growth* **69** (1984) 281.
- [22] S. Rajendran and W.R. Wilcox, *J.Crystal Growth* **69** (1984) 62.
- [23] K. Graszka, "Mass and Heat Transfer in Crystal Growth", in: ed. K. Sangwal, "Elementary Crystal Growth" (SAAN, Lublin 1994).
- [24] A. E. Turner, R. L. Gunshor and S. Datta. *Applied Optics* **22**, 3152 (1983).
- [25] F. T. J. Smith. *Metall. Trans.* **1**, 617 (1970).
- [26] Y. Marfaing. *Rev. Phys. Appl.* **12**, 211 (1977).